Brain Structure and Function
https://doi.org/10.1007/s00429-019-01838-4

ORIGINAL ARTICLE

Converging measures of neural change at the microstructural, informational, and cortical network levels in the hippocampus during the learning of the structure of organic compounds

Marcel Adam Just[1] · **Timothy A. Keller**[1]

Received: 24 July 2018 / Accepted: 21 January 2019

Abstract
The critical role of the hippocampus in human learning has been illuminated by neuroimaging studies that increasingly improve the detail with which hippocampal function is understood. However, the hippocampal information developed with different types of imaging technologies is seldom integrated within a single investigation of the neural changes that occur during learning. Here, we show three different ways in which a small hippocampal region changes as the structures and names of a set of organic compounds are being learned, reflecting changes at the microstructural, informational, and cortical network levels. The microstructural changes are sensed using measures of water diffusivity. The informational changes are assessed using machine learning of the neural representations of organic compounds as they are encoded in the fMRI-measured activation levels of a set of hippocampal voxels. The changes in cortical networks are measured in terms of the functional connectivity between hippocampus and parietal regions. The co-location of these three hippocampal changes reflects that structure's involvement in learning at all three levels of explanation, consistent with the multiple ways in which learning brings about neural change.

Keywords Diffusion imaging · fMRI · Functional connectivity · Learning · Hippocampus · Multi-voxel pattern analysis

Introduction

Learning is one of the most complex and yet fundamental processes that underlie human capabilities, enabling the acquisition of a huge amount of various types of knowledge over a lifetime. Here, we describe the phenomenon of learning in a real-world task (learning organic molecular structures) in terms of three types of brain changes in approximately 1.3 cm^3 of the left hippocampus. Different brain imaging modalities sensed three types of changes that occurred in this volume as a result of the learning: microstructural changes in tissues, informational changes (referring to encodings of the structure of individual organic molecules), and network-level synchronization changes (referring to organization among brain subsystems). The three concomitant changes in the same hippocampal locations reflect the anatomical, informational, and organizational brain changes that occur with learning.

One of the challenges of understanding the neural basis of learning is that it can be described at several scales of time and space. Our study describes brain changes that occur over the course of approximately 40 min and over volumes from 1 mm^3 to distances of about 10 cm (between the hippocampus and the parietal regions). This type of description is referred to as multimodal, in the sense that multiple brain imaging modalities (types) are used for the different characterizations. Notably, the three descriptions here all refer to the same neural tissues or brain locations. The multiple modalities all converge on a small distributed region of about 1.3 cm^3; we use 22 functional $3 \times 3 \times 6$-mm voxels for decoding in the hippocampus, where all three types of changes can be observed. This convergence results in a multilevel neural description of learning as people study molecular structures that can occur in an organic chemistry course.

The hippocampus is strongly associated with spatial navigation and memory and the formation of cognitive maps, including fine-grain information about its place cells and

✉ Timothy A. Keller
tk37@andrew.cmu.edu

[1] Department of Psychology, Center for Cognitive Brain Imaging, Carnegie Mellon University, 5000 Forbes Ave., Pittsburgh, PA 15213, USA

Published online: 06 February 2019

grid cells (e.g., Morris et al. 1982; O'Keefe and Nadel 1978). Numerous fMRI studies have reported activation of the hippocampus during tasks that require spatial memory (e.g., Brown et al. 2014), although it is uncertain whether spatial processing in the absence of a mnemonic component involves the hippocampus (Kim et al. 2015). Structural differences (enlargement) in the hippocampus have been reported to be associated with spatial memory abilities or tasks. Maguire et al. (2000) showed that the posterior hippocampi of London taxi drivers with extensive navigation experience were larger than those of control participants.

Microstructural changes in hippocampus with learning

Recent research has used MR diffusion imaging to detect short-term microstructural changes in the hippocampus resulting from spatial learning in both animals and humans (Blumenfeld-Katzir et al. 2011; Keller and Just 2016; Sagi et al. 2012; Tavor et al. 2013). The studies in humans have all shown decreases in mean diffusivity (MD) in the left but not the right hippocampus (although Sagi et al. 2012 did find MD decreases in the right parahippocampal gyrus). Although the physiological changes that could produce these changes in diffusion measures remain to be fully explored, the findings in rodents suggest that they are quantitatively associated with cellular biomarkers of synaptic change [synaptophysin (SYN)], astrocytic change [glial fibrillary acidic protein (GFAP)], and long-term potentiation [brain-derived neurotrophic factor (BDNF)]. We expected to detect such hippocampal changes during the learning of the structure of organic compounds. Furthermore, we expected these microstructural changes to occur in the same hippocampal locations as changes in network synchronization and changes in informational content.

Network-level changes with learning

Another neural property sensed by a magnetic-resonance modality is the synchronization of activation across distal brain regions [or functional connectivity, (FC)], providing a measure of the functional connectomics of the nodes of large scale brain networks (Biswal et al. 1995; Buchel et al. 1999). The role of the hippocampus in memory consolidation requires coordination with other brain regions in a large-scale network. During such consolidation, the functional connectivity between the hippocampus and the other regions provides an index of such processing (van Kesteren et al. 2010). Increases in task-related FC are thought to reflect dynamic functional changes in inter-regional communication across networks of areas and could therefore result from short-term physiological and structural neuroplastic changes (e.g., LTP, synaptogenesis, astrocyte signaling). For example, Mack and colleagues (Mack et al. 2016) found increased FC between hippocampus and several frontal regions during concept updating. In the current study, a hippocampal region showing microstructural change might be expected to also show a change in FC with other regions involved in learning the structure of organic compounds.

Changes in the neural representation of concepts

A third MR-based capability makes it possible to identify the activation of a concept (such as apple or hammer) from its fMRI signature, by applying multivoxel pattern analysis (MVPA) or machine learning to fMRI brain imaging data (Mitchell et al. 2008; Just et al. 2010). Among several domains of concepts to which this approach has been applied, such as emotions, quantities, and social interactions, the most relevant here is the study of physics concepts (Mason and Just 2016). It is possible to identify a physics concept such as gravity or frequency from its fMRI signature, and furthermore, the neural representation of a given concept is similar across all participants. Thus it should be possible to observe the neural emergence of a new concept of an organic compound. It would be particularly significant if a new neural concept emerged at the hippocampal location that showed microstructural changes and a network connectivity change.

The ability to decode some of the informational content of the hippocampus has been demonstrated in several previous studies. Chadwick et al. (2010) demonstrated the ability to decode which of three events was being recalled by applying a classifier to the activation levels of hippocampal voxels. Bonnici et al. (2012) used MVPA to show that CA1 and CA3 played a greater role in pattern completion than did other hippocampal subregions. Mack and Preston (2016) used MVPA to show that hippocampal representations are updated as additional knowledge about them is acquired. It is clear that conceptual content can be decoded from hippocampus using MVPA.

The present study collected the data necessary to examine each of these neuroimaging metrics of learning in a single 1-h MRI scanning session, focusing on the role of the hippocampus and its change in structure, information representation, and connectivity during paired-associate learning that had direct relevance to science education. The items to be learned were selected to have ecological validity for the typical introductory organic chemistry courses taught in high-school and college settings. Although some previous work has combined MVPA decoding and functional connectivity analyses to examine paired-associate learning in the hippocampus (e.g., Mack and Preston 2016; Schlichting and Preston 2014; Schlichting et al. 2015), these have all involved arbitrary pairings of visually presented objects with other objects, with faces, or with natural scenes. A recent

study examined paired-associate learning of real words and previously unknown objects (pictures of types of flowers) using changes in diffusivity to track learning. The learning task in this case is educationally relevant, although the authors did not collect fMRI data in addition to the diffusion data. Here we combine an educationally relevant task with acquisition of both BOLD fMRI data and diffusion data at multiple time points so that diffusivity changes, MVPA changes, and functional connectivity changes can all be examined simultaneously. The stimuli were 2D depictions of 3D visuospatial representations (colored sphere-and-rod models) of compounds studied in such settings. The learning involved the acquisition of the relationship between the visuospatial representations of molecules and their verbal labels used in the International Union of Pure and Applied Chemistry (IUPAC) nomenclature. An advantage of these stimuli is that there is a morpho-semantic relationship between the words and the molecular structures when considered across items, which may contribute to faster learning and allow us to detect neuroplastic changes within a single scanning session.

The hypotheses tested in the experiment include (1) microstructural changes in the left hippocampus will occur with learning in a scientific domain; (2) functional connectivity (FC) will increase with learning between the region of microstructural change in the left hippocampus and neocortical regions; and (3) when a classifier is trained only on the initial perception of the to be learned spatial representations of the compounds, it will be able to reliably classify the compounds by their retrieved fMRI signature in left hippocampus.

Materials and methods

Participants

Ten right-handed adults (9 females, 1 male between the ages of 19 and 37, mean = 24.7 years, SD = 5.2 years, 1 African American, 9 Caucasian) from the Carnegie Mellon University community participated. All participants gave signed informed consent approved by the Carnegie Mellon Institutional Review Board. None of the participants had taken an Organic Chemistry course and were consequently unfamiliar with the structure and naming system of the organic compounds presented during the study.

Although the sample size is modest, the findings from a similar paired-associate learning task that suggested that the effect size of changes in diffusivity within gray matter are quite large and consistent across participants. Hoffstetter et al. (2017) acquired data from 15 participants, and our calculation of Cohen's *d* based on the percentage changes and standard errors for the reliable percentage decreases in diffusivity reported in Table 1 of Hoffstetter et al. (2017) suggested that effect sizes between 1.2 and 1.4 were obtained, much higher than the $d = 0.8$ criteria that Cohen (1969) suggested for considering an effect to be "large". This indicates that sample size required to detect such effects with 80% power at $p < .05$ would be from 8–9 participants for a two-tailed *t* test.

Experimental paradigm

The nine organic compound images used in this experiment were originally taken from http://www.openmolecules.org. Images were then adapted to more clearly display their physical characteristics and to eliminate potential distracting aspects of each graphic. The names of the compounds had a systematic relation to the compound structures, but this systematicity was not described to the participants. [The prefix (eth-, prop-, but-) describes the number of carbon atoms present in a given molecule. The suffix (-ane, -ol, -oic acid) reflects how many oxygen atoms are present and how they bond to carbon and hydrogen atoms in the compound.]

MRI session

Each participant completed a series of different tasks involving the visualization or learning of each of the organic compounds. Participants first completed a pre-learning exposure phase. During this phase participants were presented with each picture of the organic compounds without their names. This phase provided the unlabeled neural representation of the structure of each of the compounds. Each picture was presented for 3 s for a total of six repetitions, during which the participant attended to each compound and familiarized themselves with their structure. This was followed by a 7-s rest period during which the participant fixated on an "X" displayed in the center of the screen. There were three additional presentations of a fixation "X", 17 s each, distributed across the session to provide a baseline measure.

Following the pre-learning exposure, participants performed a sequence of three separate activities, a sequence through which they would iterate two times. The first of these activities was a learning phase in which each of the compound structures was shown paired with its name. Participants were instructed to learn the pairing of the compound names with the pictures of the structures.

After each block of the learning phase, participants were tested for their retention of the picture–name pairs. Each compound name was first presented for 1 s followed by a compound picture presented for 2 s. While the picture was on the screen, participants were told to indicate whether the name and picture were correctly or incorrectly paired, using two single button mice held by the participant in the scanner.

Participants completed two learning phase blocks and two name–picture retention test periods per block of study tasks.

After completing two iterations of a learning phase and a testing phase, participants performed a post-learning cued retrieval task. The name of the compound was the cue (presented for 3 s), during which time participants were asked to visualize (retrieve) the structure of the corresponding compound. This was followed by a 7-s rest period during which the participant fixated on an "X". The set of compound names was presented six times in different random orders. There were three additional presentations of a fixation "X", 17 s each, distributed across the session to provide a baseline measure. This sequence of a learning phase, testing phase, and post-learning visualization phase was completed by each participant twice. Figure 1 provides a schematic of the experimental session.

Image acquisition

All neuroimaging data were acquired on a Siemens Verio (Erlangen, Germany) 3.0 T scanner at the Scientific Imaging and Brain Research Center of Carnegie Mellon University with a 32-channel Siemens receive coil. Diffusion-weighted structural images were acquired using the multi-band sequences (version R011 for Syngo VB17A) provided by the University of Minnesota Center for Magnetic Resonance Research (https://www.cmrr.umn.edu/multiband/). Diffusion-weighted and functional images were all collected as oblique-axial scans aligned with the anterior commissure–posterior commissure (AC–PC) line at midline.

The diffusion-weighted images were collected with the monopolar cmrr_mbep2d_diff sequence (http://www.cmrr.umn.edu/multiband) in 54 slices (an ascending interleaved acquisition with 2.4-mm-thick slices and no inter-slice gap). The matrix was 96 × 96 and FOV was 230 mm, resulting in 2.4-mm isotropic voxels (TR = 2264 ms, TE = 74.8 ms, multi-band acceleration factor = 3, number of diffusion encoded directions = 30, diffusion *b* value = 1000 s/mm^2, number of non-diffusion-encoded images = 4, bandwidth = 1860 Hz/pixel, partial Fourier factor of 6/8). The 30 diffusion encoding vectors were taken from standard Siemens gradient table. Three sets of these images were collected for each participant in the scanning session (one before the learning and again following each learning phase) with opposite phase encoding directions [anterior to posterior (AP) and posterior to anterior (PA)] so that geometric distortions and eddy currents could be corrected using FSL v. 5.0 tools (topup and eddy). The total acquisition time for these two scans was 3 min and 20 s. Each scanning session involved several functional scans using a gradient-echo echo-planar imaging pulse sequence with a repetition time of 1000 ms, echo time of 25 ms, and a flip angle of 60°. Twenty 5-mm slices, aligned along the anterior commissure–posterior commissure line, were imaged with a 1-mm interslice gap and a 32-channel head coil. The acquisition matrix was 64 × 64 with 3.125- × 3.125- × 5.0-mm in-plane resolution. Although this resolution of the functional data is somewhat coarser than that of the diffusion data, we have previously found this resolution to work well for machine learning classification (e.g., Just et al. 2010; Mitchell et al. 2008). Our choice of a lower resolution the fMRI acquisition was motivated not only by the benefit of higher signal to noise ratio for decoding the neural signatures of the compounds (by virtue of aggregating over a larger voxel volume), but also by the desire for higher temporal resolution for the functional connectivity analyses. Images were corrected for slice acquisition timing, motion, and linear trend, and they were normalized to the Montreal Neurological Institute template without changing voxel size (3.125 × 3.125 × 6 mm). There were various numbers of images acquired for each type of functional scan. The pre-exposure and post-learning retrieval tasks involved the acquisition of 605 images over 10 min,

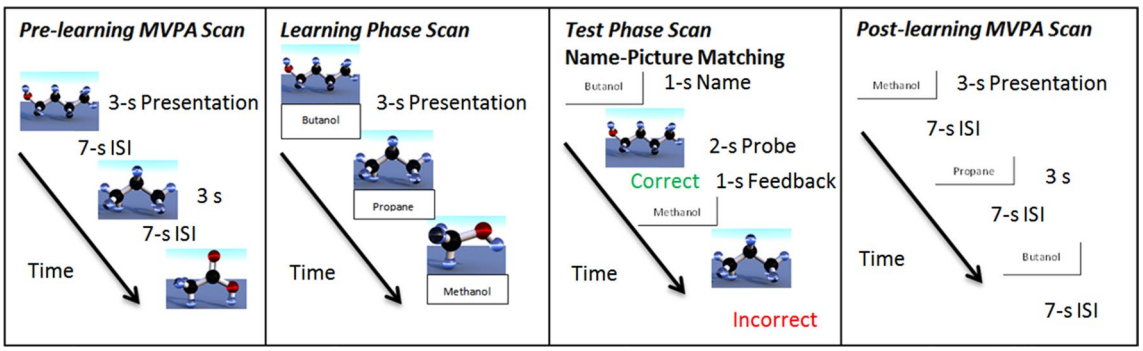

Fig. 1 Design of fMRI paradigm for the study. Participants were first exposed only to the pictures of hydrocarbon compounds, and data from the 7-s ISI was used to classify which item they were seeing. This was followed by presentation of the names with the pictures, and a test phase requiring them to decide if a picture corresponded to the preceding compound name. Participants then saw only the names and were instructed to retrieve and imagine an image of the compound during the delay interval. The learn-test-retrieve phases were repeated twice

5 s. The two in-scanner learning-phase sessions involved the collection of 198 images over 3 min, 18 s.

Image processing and analysis

To allow comparison across imaging modalities, sessions, and participants a number of precise pre-processing corrections and co-registrations of the imaging data were required. Preprocessing of the diffusion-weighted images (DWI) made use of tools from FSL v. 5.0.8 (http://fsl.fmrib.ox.ac.uk/fsl/fslwiki/) (Smith et al. 2004), and code written in-house for motion correction of diffusion data (Jung 2010; Jung et al. 2013) running under MATLAB®, v. R2011a (http://www.mathworks.com/products/matlab). Brain-only masks of images at each stage of the following procedures were extracted using the FSL's "bet2". Estimation and correction of geometric distortion was carried out for each session (pre-training and post-training) using the eight non-diffusion-weighted images (b value = 0), four collected with each phase encoding direction (A > P, P > A) (Andersson et al. 2003). FSL's "topup" tool was first used to estimate a warp-field and the data were subsequently resliced and the two diffusion runs averaged using the "applytopup" tool. FSL's "eddy" tool was then used to simultaneously model the eddy current effects and head motion effects in the run-averaged data using default values for all parameters (i.e., a quadratic spatial model, no spatial filtering, and five iterations of the non-linear estimation).

Additional pre-processing involved generation of an estimated diffusion-weighted image for each corrected diffusion-weighted image on the basis of average signal intensities across the corrected un-weighted (b value = 0) images, a method proposed by Bai and Alexander (2008) and shown to improve the co-registration of diffusion-weighted data collected with even relatively low b values (1200 s/mm^2). This is similar to the well-known UNDISTORT (Using Non-Distorted Images to Simulate a Template of the Registration Target) method proposed by Ben-Amitay et al. (2012), except that a simple diffusion tensor model is used rather than the more complex Composite Hindered and Restricted Model of Diffusion (CHARMED) proposed by Assaf and Basser (2005). It is also essentially the same as a method proposed by Nam and Park (2011) that used a diffusion tensor model to simulate the high b value image templates, but also incorporated a non-linear registration method for the motion correction. The estimation and reslicing was carried out with FSL's "mcflirt" program, using a correlation ratio cost function. Finally, each of the affine transformation matrices computed above were combined, and a single reslicing of the original data was carried out with FSL's "applywarp" and the direction of the diffusion vectors were rotated on the basis of this combined transformation prior to fitting a weighted-least squared diffusion tensor model with FSL's "dtifit."

An additional co-registration was required to compare the before and after repeated measures of DTI metrics within each participant. The fractional anisotropy (FA) images calculated for each session provide exquisite contrast for carrying out this co-registration and so these were used in preference to the mean of the un-weighted (b value = 0) images, and because FA is a normalized measure (the standard deviation of three eigenvalues from the DTI fit), changes in signal due to scanner drift between acquisitions can be ignored. Specifically, a forward (pre- to post-training) and backward (post- to pre-training) 12-parameter affine transformation matrix was calculated with FSL's "flirt" for each participant's two FA images, and the half-way transformation matrix of each was used to re-slice the data into a position half-way between the two FA images. This method ensures that both the pre- and post-training images undergo comparable spatial blurring during the re-slicing process.

To allow comparison across participants, we used FSL's "fnirt" tool with default parameters for FA to FA non-linear co-registration, to estimate the warping from each participant's pre- and post-training FA map to the FMRIB_FA_1 mm template included in FSL. This non-linear warping was applied to each participant's mean diffusivity image (the average of the three eigenvalues resulting from the tensor fit). Following the initial transformation to the FMRIB_FA_1 mm template, a study specific template was created by averaging all FA data from both groups and both sessions, and this was used as the target for final non-linear spatial normalization of each FA image. These final warp coefficients were then applied to the mean diffusivity maps for each participant. In contrast to the approach used to compare FA across participants using Tract-based Spatial Statistics (Smith et al. 2006), instead of projecting the diffusivity data to the white matter skeleton defined by peak FA, we used a voxel-wise analysis restricted to the left and right hippocampus [as defined by the automated anatomical labeling (AAL) atlas]. The specific hypothesis that structural changes in the form of decreased MD would be found in the left hippocampus was tested by calculating voxel-wise changes in this region of interest (and separately in the right hippocampus for comparison). Analysis of changes in mean diffusivity within these regions was then tested by comparing pre- and post-training data as a paired t test across all participants family wise-error-corrected for multiple comparisons using Gaussian random field theory and the cluster extent threshold with a cluster forming t threshold of 2.00.

Pre-processing of the T2*-weighted EPI data was carried out with a combination of tools from MATLAB® v. R2011a, SPM12, and FSL v. 5.0.8. Because the position of the head was not perfectly aligned between sessions, we first corrected each run separately for geometric

distortions using the gradient-echo field map collected within the same session and FSL's "prelude" and "fugue" tools. Motion was then estimated separately within each run with FSL's "mcflirt" using default (six-parameter affine) co-registration, reference as the temporally middle volume acquired, normalized correlation cost functions settings (Jenkinson et al. 2002), and the "fsl_motion_outliers" script was used to calculate the temporal derivative of the root-mean-square variance (DVARs) (Power et al. 2012) between each image and the next. Motion outliers were identified as any point with a DVAR value greater that the 75th percentile + 1.5 times the interquartile range. Indices for images considered outliers were saved in a regressor so that their effect could be removed (i.e., "scrubbed") prior to functional connectivity analyses.

To allow comparison across sessions, a co-registration strategy similar to that used for the DWI data was carried out. The mean of each motion corrected fMRI run was used to calculate a forward (pre- to post-training) and backward (post- to pre-training) six-parameter affine transformation matrix with FSL's "flirt" tool. The halfway transformation matrix of each was then saved to later re-slice the data into a position half-way between the two means. These means were averaged for each participant and a non-linear transformation between each participant's mean EPI image and the MNI averaged 152-participant T2-weighted template was carried out using FSL's "fnirt" tool with default registration schedule parameters for intramodal T2-weighted registration. All participants' data were then averaged to create a study specific EPI template, and the transformation from the participant's mean to this new template was saved as the final non-linear warping. (Note that final re-slicing of the data was all done in a single step that concatenated all the pre-calculated transformation matrices together and used a final sync interpolation to an MNI space with the same resolution as the acquired functional data.)

For the analysis of functional connectivity, a region of interest was defined taking the 100 1-mm^3 voxels from the diffusion data showing the largest decrease in mean diffusivity for each participant distributed throughout the AAL-defined left hippocampus. The averaged time-series of all voxels within each region of interest defined by the automated anatomical labeling (AAL) atlas (Tzourio-Mazoyer et al. 2002) were also calculated for each participant, and all pairwise correlations were calculated among regions of interest, Fisher-z-transformed, and submitted to a group paired t test. The analysis of intrinsic functional connectivity was identical, except that spatially normalized data were band pass filtered using FSL's "fslmaths" tool, retaining frequencies between approximately 0.01 Hz (high-pass sigma = 50) and 0.1 Hz (low-pass sigma = 5).

MVPA classification

The percentage signal change relative to the fixation condition was computed at each gray-matter voxel for each stimulus presentation. The main input measure for the subsequent analyses consisted of the mean activation level over the six brain images acquired within a 4-s window, offset 6 s from the stimulus onset (to account for the delay in hemodynamic response). The percentage signal-change data of the voxels in the mean image for each word were then converted to z-scores.

A critical step in multi-voxel pattern analysis is the selection of a relatively small set of voxels likely to provide systematic information about the identity of the neural representation that is active without contributing additional noise. The approach to selection taken here was to first identify those voxels that are stable across the multiple presentations of the set of items, and then to select from within the most stable voxels those that show evidence of microstructural change. Voxel stability is measured by the correlation of activation across the set of items and averaged over the multiple pairs of presentations. High stability is thus an analytic for the replicability of the voxel's activity in its participation in the neural representation of the item. The voxel selection is based on only the classifier's training data for the model in each cross-validation fold and is then applied to the test data.

The multivoxel pattern analyses used a Gaussian Naïve Bayes (GNB) classifier (using pooled variance) (support vector machine classifiers were also explored but found to provide no significant advantage in item classification). The classifier here is a mapping function f of the form f: voxel activation levels $X_1, \ldots, X_n \rightarrow Y_i$, $i = 1, \ldots, m$, where Y_i are stimulus items and where voxel activation levels are mean activation levels of the selected voxels. GNB is a discriminative classifier that models the joint distribution of class Y and attributes $X_1, \ldots, X_n$, which are conditionally independent given Y. The rank accuracy (hereafter, simply "accuracy") of the classification is the normalized rank of the correct label in the classifier's posterior-probability-ordered list of classes. If the classifier were operating at chance, the correct label would on average appear in the middle of the ranked list, producing a chance level accuracy of 0.50. Accuracies are calculated for each item in each fold and then averaged across folds, and then across items. The cutoff for determining whether rank accuracy exceeds that expected by chance are obtained using Monte Carlo testing with 10,000 randomly generated data sets given the number of items and the number of folds, and performing the same calculations to obtain a normal probability distribution with mu and sigma estimated from the random data. The machine learning establishes a measure of the correspondence between the stimulus items and the activation patterns.

Results

All data were collected in a single scanning session. Diffusion-weighted MRI data were collected prior to training, and following each of the two testing sessions. Functional MRI data were collected during each phase in a single scanning session, and the cycle of training, testing, and retrieving the visuo-spatial representation of the compound when provided with only the names was repeated twice following pre-exposure to the stimuli.

Microstructural changes in hippocampus following learning, assessed with diffusion-weighted imaging

A region of the left hippocampus showed a reliable decrease in mean diffusivity (MD) between the pre-learning and post-learning DTI scans [peak $t(9) = 2.72$, $p < .5$, corrected for cluster extent at a height threshold of $t = 2.00$]. The center of mass of the change was at MNI coordinates −25, −18, −16. This cluster is approximately 420 mm^3 in volume or 13% of the L hippocampus and is shown in Fig. 2. This location is approximately 1 cm more posterior and superior to the one previously found following spatial route learning (e.g., Keller and Just 2016; Sagi et al. 2012). The location of this changed region can be localized probabilistically to different L. hippocampal subregions using the Juelich Histological atlas in FSL v.5.0, resulting in a probability of 57% for CA, 50% for the dentate gyrus, 34% for the subiculum.

As noted in the methods, our modest sample size was still estimated to be large enough to detect the size of effects found for gray matter diffusivity changes following learning in a recent study (Hoffstetter et al. 2017). For the present data, a post hoc power analysis yielded a similarly large effect size. Cohen's *d* (adjusted for a paired *t* test by the method recommended by Dunlop et al. (1996), was 1.15, indicating that for 80% power at $p < .05$ for a one tailed test, we should have planned to test at least seven participants). Unlike many conventional fMRI studies, our analyses of changes in mean diffusivity seem to benefit from relatively low variability across participants compared to the relatively large decreases in MD that can be induced by learning.

We acquired the DWI data at a higher spatial resolution than the fMRI data upon which the remaining analyses were based to maximize the possibility of isolating which of the anatomically differentiable hippocampal regions were affected by the neuroplasticity. To verify that we obtained similar results when the diffusion data were resliced to match the resolution of the fMRI data, we carried out the same analysis of the diffusion data with spatial normalization performed using the version of the MNI template resampled to match the acquired resolution of the functional data. The results were similar to those reported above, although the location of the largest group difference in MD was slightly more anterior and inferior to that found with the higher resolution data [MNI coordinates −28, −9, −20; $t(9) = 2.54$, $p < .05$].

Informational changes in hippocampus following learning, assessed with MVPA classification

If the neural representations of the stimulus compound structures become differentiated with learning, then a classifier should be able to identify which item was being cued (by the item's name) when the item structure was retrieved. A Gaussian naïve Bayes classifier was trained only on fMRI data from the pre-learning picture presentation blocks at the beginning of the study (which established the neural representation of each item's structure before any item names were introduced). The classifier was then tested on its ability to identify the neural representation of each item's structure

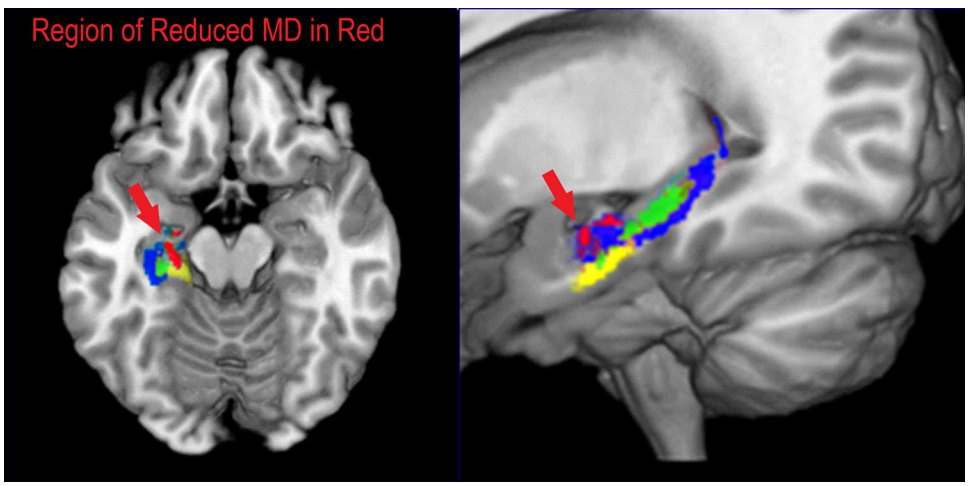

Fig. 2 Region of left hippocampus (in red) showing decreased mean diffusivity (MD) after learning. Hippocampal subregions: CA shown in blue; dentate gyrus in green; subiculum in yellow

during the last post-learning test phase when participants were cued with only the item name.

To test whether the same left hippocampal region that showed a diffusivity change also encoded the learned association (between the item's name and its structure), the voxels for MVPA classification were selected for each individual participant by considering the 100 1-mm^3 voxels in that participant's left hippocampus that had the highest mean diffusivity decrease with learning. The features selected for use in classification were any $3.125 \times 3.125 \times 6$ mm functional (fMRI) voxel that contained one or more of the 100 1-mm^3 voxels whose mean diffusivity had decreased most. This resulted in a selection of a mean of 22.2 functional voxels per participant (range 16–30) which constitutes a mean volume of 1.3 cm^3 or about 40% of the total L. hippocampal volume. To verify that these selected features (functional voxels) were predominantly co-located with the area of decreased MD in the left hippocampus in the group analysis of the diffusion data, we constructed of "hit-map" of the functional voxels selected across all participants and calculated the overlap between these voxels and the region of decreased MD shown in Fig. 2. The volume of the functional voxels selected for at least 4 of the 10 participants was 820 mm^3 and their overlap with the 420 mm^3 region of decreased MD in the group analysis was nearly complete (410 mm^3 of shared tissue). The temporal window within which the activation of these functional voxels was analyzed spanned from 6 to 9 s after stimulus onset.

The classification accuracy after the second iteration of learning using these voxels in the left hippocampus with decreased mean diffusivity produced a rank accuracy of 0.57, reliably above chance level ($p < .05$), as shown in Fig. 3. This result shows that retrieved mnemonic representations of the structure of individual items can be decoded from the hippocampus, consistent with a theorized hippocampal function of pattern separation (learning distinctions between patterns). Furthermore, this classification accuracy reliably increased from the 0.48 level obtained after the first iteration of learning [$t(9) = 2.23$, $p = .05$]. In contrast, voxels selected in the same way from the right hippocampus did not result in classification accuracy above chance at either time point.

The ability to decode the retrieved structural representation of the compounds in response to the words was also examined in a number of neocortical regions that might also be involved in the neural representation of the spatial structure of the compounds (namely, superior and inferior parietal lobules, fusiform gyrus, parahippocampal gyrus, superior and inferior extrastriate occipital regions, and calcarine sulcus). The functional voxels used as features for the classification were each participant's 60 most stable voxels within each region, with regions defined by AAL parcellation (automated anatomical labeling atlas). The temporal

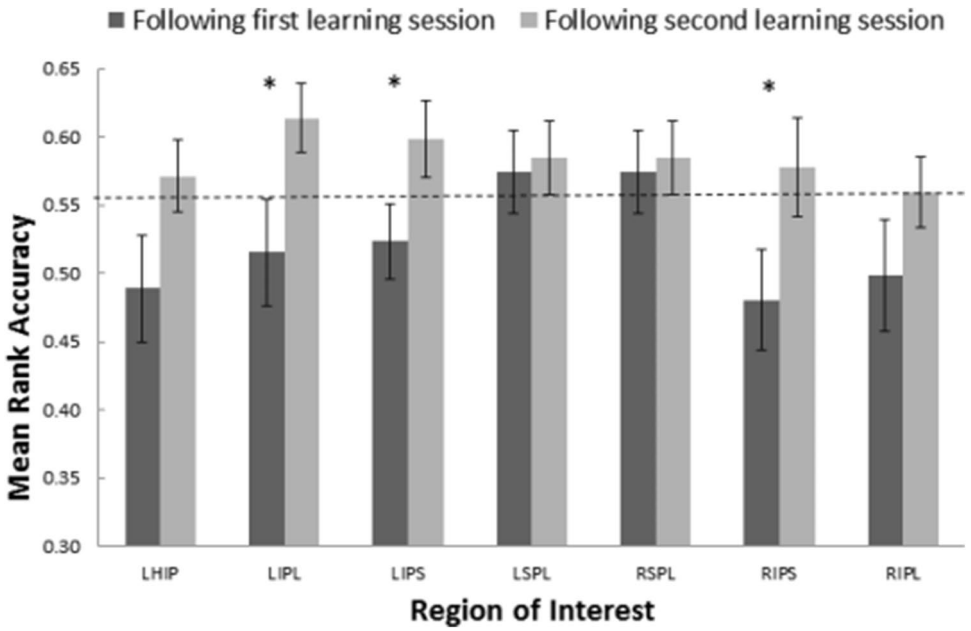

Fig. 3 Mean rank accuracy of the GNB classifier trained on only activation evoked by the initial unlabeled pictures presented prior to learning the compounds' names. The classifier then predicted which of nine molecular structures a participant was retrieving when they were given only the name of the molecule as a cue, at two time points (after first and second learning session). The $p < .05$ critical value for rank accuracy greater than chance is shown by the dashed horizontal line. Region abbreviations for regions displaying reliable classification accuracy after the second learning session: *L* and *R* hemisphere, *HIP* hippocampus, *IPS* intraparietal sulcus, *IPL* inferior parietal lobule, *SPL* superior parietal lobule. Error bars indicate standard error of the mean

window of the functional voxels in the classifier's training set spanned from 6 to 9 s post stimulus onset, and the test set used a window of 8 to 11 s. As above, the training set was based on data evoked by the unnamed pictures presented during the pre-learning phase. The test sets were acquired during the post-learning test phase, in which only the name of the compound was presented.

Three regions (L inferior parietal and L and R intraparietal sulcus), all of which are associated with spatial representation, showed a significant increase in classification accuracy between the two learning sessions [$t(9) = 2.76$; $t(9) = 2.41$; $t(9) = 2.67$, respectively, p values $< .05$, 1-tailed t tests] as shown in Fig. 3. (There was also a reliable overall main effect of learning session [$F(1, 9) = 7.65$, $p < .05$].) After the second block of learning, L hippocampus and 6 parietal areas (left and right inferior, superior, and intraparietal) showed rank classification accuracy above chance, as shown in Fig. 3. Thus, the molecular structure of the compounds can be reliably decoded from the L hippocampus and from several parietal regions after two iterations of learning trials.

Functional connectivity changes involving hippocampus, assessed with task-based fMRI

There is typically an increase in inter-regional functional connectivity (increased synchronization of activation in involved regions) with learning (Büchel et al. 1999; Schipul et al. 2012). The analysis here tested whether the same left hippocampal voxels that showed a mean diffusivity change and an informational change were also involved in binding together the activity of learning-relevant neocortical areas. (The learning-relevant areas are assumed to be those that contain the neural representations of the molecular structures of the organic compounds, as revealed by the MVPA analyses above.) The hippocampal voxels within each participant with the largest mean diffusivity change should show an increase in functional connectivity with these regions between the time of the initial baseline picture presentations (when participants did not know the item names), and the time of the scans following the learning trials (when participants were actively attempting to visualize the molecular structure given the name). We therefore compared the functional connectivity between these individually chosen left hippocampal voxels and the six parietal regions that showed a reliable classification accuracy. Four of these six parietal regions showed a reliable increase in their functional connectivity with the hippocampal region after the initial block of learning, namely left inferior parietal [L IPL, $t(9) = 2.99$], left superior parietal [L SPL, $t(9) = 3.19$], left intraparietal sulcus [L IPS, $t(9) = 3.19$], and right intraparietal sulcus [R IPS, $t(9) = 3.38$], (all $p < .05$). (The other 2 regions showed a non-reliable increase.) Thus, the microstructurally altered voxels of the left hippocampus establish heightened synchronization with bi-lateral parietal regions associated with spatial processing. The functional connectivity increased from the time before the association between the item names and item structures were known, to the time when they had been learned. Notably, a similar analysis of connectivity between voxels in the right hippocampus showing the largest decrease in diffusivity and these bilateral parietal regions showed no change in synchronization of activation, indicating a clear hemispheric difference in the spatial specificity of the diffusion and connectivity changes.

In addition to the increase in the task-related FC between the left hippocampal region of microstructural change and parietal regions, there was also an increase in the intrinsic connectivity between the left hippocampal region of MD decrease and these parietal regions. This result was obtained by performing a similar analysis on the same data which was low-pass filtered at 0.1 Hz. In this analysis there were significant increases in intrinsic connectivity with the left superior parietal lobule [L SPL, $t(9) = 3.18$, $p < .05$], and the right superior parietal lobule [R SPL, $t(9) = 2.92$, $p < .05$]. [There were also trends toward similar increases in intrinsic connectivity with the left and right inferior parietal lobules $t(9) = 2.10$, $p < .10$, and $t(9) = 2.22$, $p < .10$, respectively.]

Behavioral measure of learning

The multiple converging neural measures of learning described above corresponded well to the behaviorally measured learning of the association between the names and the structures of the molecules. After the second learning session, the mean performance was 87.8% correct (8 out of 9 items correct). The increase in behavioral accuracy over learning blocks was approximately linear ($R^2 = 0.99$), as shown in Fig. 4, and the increase was reliable [$F(3,27) = 5.86$, $p < .005$]. Reaction times for the behavioral judgments also decreased monotonically across the four test blocks and the decrease was well-fit by a power function ($R^2 = 0.89$).

Discussion

The study found three types of neural changes in the same brain tissues (~ 1.3 cm^3) in the left hippocampus while participants reliably learned to associate the spatial configuration of a set of organic compounds with their names. The informational change concerning the retrieved structure of individual compounds came to be present in distributed left hippocampal locations, indicated by the classifier's ability to reliably identify the organic molecule on the basis of its retrieved spatial configuration (when participants were prompted by only the compound's name).

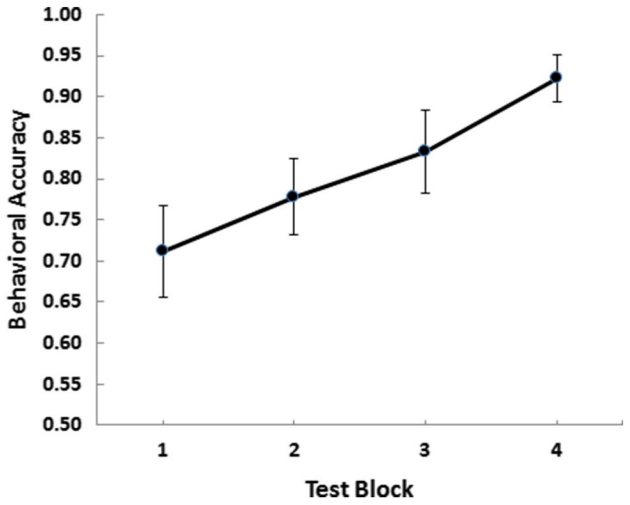

Fig. 4 Mean behavioral accuracy in the test blocks of the experiment. Blocks 1 and 2 were completed prior to the first post-learning MVPA and blocks 3 and 4 were completed between he first and second post-learning MVPA scans. Error bars indicate standard error of the mean

This outcome is similar to several previous findings of hippocampal informational change with learning (e.g., Mack and Preston 2016). During the same learning period of 40 min and within a similar gray matter location, the mean diffusivity reliably decreased, indicating that microstructural neuroplastic changes in the dentate gyrus and CA were occurring. Such microstructural changes play a role in consolidating the learned information. A third type of change occurring during this same time period and at the same locations was the change in functional connections that were being established to other cortical regions. The co-location of these three types of neural changes during concept learning indicates the centrality of small portions of the left hippocampus in the neural establishing of usable new knowledge of the spatial properties of a concept, and also illustrates some of the learning mechanisms that are involved.

The decoding of individual compounds from the hippocampus demonstrates two of this region's main postulated functions: pattern separation and pattern completion (Marr 1971). The finding that a classifier can differentiate among the nine different compounds provides evidence of pattern separation, the distinctive encoding of similar learning episodes, allowing distinct long-term access to very similar information. This rapid encoding of ongoing episodic information is thought to be carried out by a relatively simple autoassociative network involving at least the dentate gyrus.

The ability to retrieve the spatial configuration of a compound given only its name (indicated by a classifier's ability to identify the retrieved spatial configuration of the named compound) demonstrates pattern completion. The item name was only a fragment of the activity pattern present at encoding and yet the spatial configuration activity present during the episode was retrieved.

Marr's analysis of the connection properties of different regions and different cell types within the hippocampus forms much of the basis of the current theories of how hippocampal subregions of the dentate gyrus and cornus ammonis accomplish the two necessary functions, and subsequent computational modeling of the processes has been consistent with the basic theory (e.g., O'Reilly and McClelland 1994; O'Reilly and Rudy 2000). The current findings demonstrate in detail the presence of the postulated pattern separation function in the dentate gyrus.

Functional imaging has supported the idea that dorsal hippocampus including the dentate gyrus and CA3, is primarily involved in pattern separation, and that the ventral hippocampus including the subiculum and CA1 is relatively more involved in pattern completion (Bakker et al. 2008; Lacy et al. 2010; Yassa and Stark 2011). High-resolution fMRI of the hippocampus has allowed MVPA methods to be applied to these separate hippocampal fields has attempted to provide more fine-grain dissociations and suggests that the dentate gyrus and CA3 are specialized for pattern separation and that CA1 is more likely involved in pattern completion (Berron et al. 2016; Bonnici et al. 2012). The present functional data do not allow us to distinguish these functions, likely due to the relative coarseness of the MRI resolution. However, because both functions are involved in the learning task, it is not surprising that the decrease in diffusion within the hippocampus with learning extended across both of these subfields of the hippocampus.

The MVPA/machine learning approach makes it possible to watch the neural representations of new concepts grow in the brains of learners as the concepts are being acquired (Bauer and Just 2015). The neural representations become more distinct and identifiable as participants gain additional exposure to the concepts. This capability opens the possibility of investigating the neural acquisition of individual new STEM concepts, to determine which facets of the learning and instruction may be amenable to enhancement.

The ability to identify the neural representation of a new concept as it is being learned opens the possibility of cognitive neuroscience findings informing and enhancing instructional methods. It is possible to assess several different types of neural properties of concept representations in STEM learners, and to determine how these properties are related to behavioral indices of learning. One example is that a given participant's neural representations of a set of key concepts can be compared to those of a successful advanced student, to determine whether neural similarity is an accurate predictor of academic mastery of the concepts. Another example is that the intrinsic reliability and identifiability of a participant's neural representations might be predictive of academic mastery of the concepts. A third possibility is

that the dimensional structure of the neural representations might analyzed with the goal of revealing which facets of the concept may be underdeveloped and maybe be enhanced with targeted additional instruction. The neural properties of a concept representation have the potential to substantially contribute to prediction of learning outcomes above and beyond what behavioral measures can predict. In the long term, it may be possible to develop combined neural and behavioral models to guide the design of in-classroom interventions that leverage the new neural data beyond classical behavioral measures.

The study leaves many interesting questions unanswered, but some of them seem readily addressable. First, it remains unclear whether the three types of neural changes in left hippocampus are specific to the learning of spatial information or whether some or all of them also occur at the same location and with similar properties with the learning of other, non-spatial types of information. Second, the left lateralization of the hippocampal neuroplasticity in this study and in previous studies is somewhat surprising. Although it could be argued that this hemispheric specificity is due to the linguistic content in the present task, that explanation is less tenable for studies showing left lateralized hippocampal changes in diffusivity after practice at non-verbal spatial memory tasks in humans (e.g., Keller and Just 2016; Tavor et al. 2013). Interestingly though, recent studies in mice have found that optogenetic stimulation differentially affects plasticity in left and right hippocampus (Kohl et al. 2011) and that optogenetic "silencing" of the left hippocampus but not the right hippocampus, impairs performance on an associative spatial memory task (Shipton et al. 2014). Third, there may also be changes in associated white matter myelination or structural integrity at the hippocampal parcel identified here, but the time frame of 40 min may be too short for such changes to be measurable. We have previously provided evidence of such myelination changes following 100 h of reading instruction (Keller and Just 2009), and Hofstetter et al. (2017) have recently shown diffusion changes in both gray and white matter following 2 h of new word learning. Finally, future work applying these methods to a wide variety of educational materials in many fields is clearly of interest.

The main focus of the findings is the integration of three types of neural changes in left hippocampus with learning. As new methods for assessing neural changes proliferate, it sometimes becomes difficult to apply multiple assessments within the same study. The three magnetic-resonance-based sensing technologies used here converge to show the co-location of these different types of neural changes. The diffusivity-based sensing of microstructural change with learning is the newest of the three modalities, and it produces, at least in this study, the finest grain of spatial granularity. To fully understand a phenomenon as complex as human learning will likely require increasingly integrated accounts of neural changes sensed in different ways.

Acknowledgements The authors thank Zachary Anderson for assistance in designing and conducting the experiment, Theodore Depietro Jr. for machine learning analyses of the data, and Vladimir Cherkassky and Robert Mason for comments on earlier versions of the manuscript.

Funding This research was supported by the Office of Naval Research (Grant number N00014-16-1-2694).

Compliance with ethical standards

Conflict of interest The authors declare that they have no conflicts of interest.

Research involving human participants All procedures performed in studies involving human participants were in accordance with the ethical standards of the institutional and/or national research committee and with the 1964 Helsinki declaration and its later amendments or comparable ethical standards.

Informed consent All participants gave signed informed written consent on a consent form approved by the Carnegie Mellon Institutional Review Board.

Ethical approval All procedures performed were approved by the Institutional Review Board of Carnegie Mellon University and were in accordance with the ethical standards of this committee and with the 1964 Helsinki declaration and its later amendments. This article does not contain any studies with animals performed by any of the authors.

References

Andersson JLR, Skare S, Ashburner J (2003) How to correct susceptibility distortions in spin-echo echo-planar images: application to diffusion tensor imaging. Neuroimage 20:870–888. https://doi.org/10.1016/S1053-8119(03)00336-7

Assaf Y, Basser PJ (2005) Composite hindered and restricted model of diffusion (CHARMED) MR imaging of the human brain. Neuroimage 27:48–58. https://doi.org/10.1016/j.neuroimage.2005.03.042

Bai Y, Alexander DC (2008) Model-based registration to correct for motion between acquisitions in diffusion MR imaging. In: 2008 IEEE international symposium on biomedical imaging: from nano to macro. Paris, France, pp 947–950

Bakker A, Kirwan CB, Miller M, Stark CEL (2008) Pattern separation in the human. Science 319:1640–1642. https://doi.org/10.1126/science.1152882

Bauer AJ, Just MA (2015) Monitoring the growth of the neural representations of new animal concepts. Hum Brain Mapp 36:3213–3226. https://doi.org/10.1002/hbm.22842

Ben-Amitay S, Jones DK, Assaf Y (2012) Motion correction and registration of high b-value diffusion weighted Images. Magn Reson Med 67:1694–1702. https://doi.org/10.1002/mrm.23186

Berron D, Schutze H, Maass A et al (2016) Strong evidence for pattern separation in human dentate gyrus. J Neurosci 36:7569–7579. https://doi.org/10.1523/JNEUROSCI.0518-16.2016

Biswal B, Yetkin FZ, Haughton VM, Hyde JS (1995) Functional connectivity in the motor cortex of resting human brain using echo-planar MRI. Magn Reson Med 34:537–541. https://doi.org/10.1002/mrm.1910340409

Blumenfeld-Katzir T, Pasternak O, Dagan M, Assaf Y (2011) Diffusion MRI of structural brain plasticity induced by a learning and memory task. PLoS One. https://doi.org/10.1371/journal.pone.0020678

Bonnici HM, Chadwick MJ, Kumaran D et al (2012) Multi-voxel pattern analysis in human hippocampal subfields. Front Hum Neurosci 6:1–13. https://doi.org/10.3389/fnhum.2012.00290

Brown TI, Hasselmo ME, Stern CE (2014) A high-resolution study of hippocampal and medial temporal lobe correlates of spatial context and prospective overlapping route memory. Hippocampus 24:819–839. https://doi.org/10.1002/hipo.22273

Büchel C, Coull JT, Friston KJ (1999) The predictive value of changes in effective connectivity for human learning. Science 283:1538–1541. https://doi.org/10.1126/science.283.5407.1538

Chadwick MJ, Hassabis D, Weiskopf N, Maguire EA (2010) Decoding individual episodic memory traces in the human hippocampus. Curr Biol 20:544–547. https://doi.org/10.1016/j.cub.2010.01.053

Cohen J (1969) Statistical power analysis for the behavioral sciences. Academic, New York

Dunlop WP, Cortina JM, Vaslow JB, Burke MJ (1996) Meta-analysis of experiments with matched groups or repeated measures designs. Psychol Methods 1:170–177

Hofstetter S, Friedmann N, Assaf Y (2017) Rapid language-related plasticity: microstructural changes in the cortex after a short session of new word learning. Brain Struct Funct 222:1231–1241. https://doi.org/10.1007/s00429-016-1273-2

Jenkinson M, Bannister P, Brady M, Smith SM (2002) Improved optimisation for the robust and accurate linear registration and motion correction of brain images. Neuroimage 17:825–841. https://doi.org/10.1006/nimg.2002.1132

Jung K-J (2010) Sensitivity of motion estimation to the anisotropic diffusion of white matter in diffusion MRI. In: Proceedings of the 18th Annual Meeting of the ISMRM. Stockholm, Sweden, p 4036

Jung K-J, Kohli N, Yeh F-C, Keller TA, Zhao T (2013) Motion correction in diffusion spectrum imaging using simulated diffusion images at multiple b bands. In: Proceedings of the 21st Annual Meeting of the ISMRM. Salt Lake City, Utah, USA, p 3192

Just MA, Cherkassky VL, Aryal S, Mitchell TM (2010) A neurosemantic theory of concrete noun representation based on the underlying brain codes. PLoS One. https://doi.org/10.1371/journal.pone.0008622

Keller TA, Just MA (2009) Altering cortical connectivity: remediation-induced changes in the white matter of poor readers. Neuron 64:624–631. https://doi.org/10.1016/j.neuron.2009.10.018

Keller TA, Just MA (2016) Structural and functional neuroplasticity in human learning of spatial routes. NeuroImage 125:256–266. https://doi.org/10.1016/j.neuroimage.2015.10.015

Kim CH, Heath CJ, Kent BA et al (2015) The role of the dorsal hippocampus in two versions of the touchscreen automated paired associates learning (PAL) task for mice. Psychopharmacology 232:3899–3910. https://doi.org/10.1007/s00213-015-3949-3

Kohl MM, Shipton OA, Deacon RM et al (2011) Hemisphere-specific optogenetic stimulation reveals left-right asymmetry of hippocampal plasticity. Nat Neurosci 14:1413–1415. https://doi.org/10.1038/nn.2915

Lacy JW, Yassa MA, Stark SM et al (2010) Distinct pattern separation related transfer functions in human CA3/dentate and CA1 revealed using high-resolution fMRI and variable mnemonic similarity. Learn Mem 18:15–18. https://doi.org/10.1101/lm.1971111

Mack ML, Preston AR (2016) Decisions about the past are guided by reinstatement of specific memories in the hippocampus and perirhinal cortex. Neuroimage 127:144–157. https://doi.org/10.1016/j.neuroimage.2015.12.015

Mack ML, Love BC, Preston AR (2016) Dynamic updating of hippocampal object representations reflects new conceptual knowledge. Proc Natl Acad Sci 113:13203–13208. https://doi.org/10.1073/pnas.1614048113

Maguire EA, Gadian DG, Johnsrude IS et al (2000) Navigation-related structural change in the hippocampi of taxi drivers. Proc Natl Acad Sci USA 97:4398–4403. https://doi.org/10.1073/pnas.070039597

Marr D (1971) Simple memory: a theory for archicortex. Philos Trans R Soc B Biol Sci 262:23–81. https://doi.org/10.1098/rstb.1971.0078

Mason RA, Just MA (2016) Neural representations of physics concepts. Psychol Sci 27:904–913. https://doi.org/10.1177/0956797616641941

Mitchell TM, Shinkareva SV, Carlson A et al (2008) Predicting human brain activity associated with the meanings of nouns. Science 320:1191–1195. https://doi.org/10.1126/science.1152876

Morris RGM, Garrud P, Rawlins JNP, O'Keefe J (1982) Place navigation impaired in rats with hippocampal lesions. Nature 297:681–683

Nam H, Park H-J (2011) Distortion correction of high b-valued and high angular resolution diffusion imagesusing iterative simulated images. Neuroimage 57:968–978. https://doi.org/10.1016/j.neuroimage.2011.05.018

O'Keefe J, Nadel L (1978) The hippocampus as a cognitive map. Oxford University Press, New York

O'Reilly RC, McClelland JL (1994) Hippocampal conjunctive encoding, storage, and recall: avoiding a trade-off. Hippocampus 4:661–682. https://doi.org/10.1002/hipo.450040605

O'Reilly RC, Rudy JW (2000) Computational principles of learning in the neocortex and hippocampus. Hippocampus 10:389–397

Power JD, Barnes KA, Snyder AZ et al (2012) Spurious but systematic correlations in functional connectivity MRI networks arise from subject motion. Neuroimage 59:2142–2154. https://doi.org/10.1016/j.neuroimage.2011.10.018

Sagi Y, Tavor I, Assaf Y (2012) Learning in the fast lane: new insights into neuroplasticity from diffusion MRI. Neuron 73:1–16

Schipul SE, Williams DL, Keller TA et al (2012) Distinctive neural processes during learning in autism. Cereb Cortex 22:937–950. https://doi.org/10.1093/cercor/bhr162

Schlichting ML, Preston AR (2014) Memory reactivation during rest. Proc Natl Acad Sci 111:15845–15850. https://doi.org/10.1073/pnas.1404396111

Schlichting ML, Mumford JA, Preston AR (2015) Learning-related representational changes reveal dissociable integration and separation signatures in the hippocampus and prefrontal cortex. Nat Commun 6:8151. https://doi.org/10.1038/ncomms9151

Shipton OA, El-Gaby M, Apergis-Schoute J et al (2014) Left–right dissociation of hippocampal memory processes in mice. Proc Natl Acad Sci 111:15238–15243

Smith SM, Jenkinson M, Woolrich MW et al (2004) Advances in functional and structural MR image analysis and implementation as FSL. Neuroimage 23:208–219. https://doi.org/10.1016/j.neuroimage.2004.07.051

Smith SM, Jenkinson M, Johansen-Berg H et al (2006) Tract-based spatial statistics: voxelwise analysis of multi-subject diffusion data. Neuroimage 31:1487–1505. https://doi.org/10.1016/j.neuroimage.2006.02.024

Tavor I, Hofstetter S, Assaf Y (2013) Micro-structural assessment of short term plasticity dynamics. Neuroimage 81:1–7. https://doi.org/10.1016/j.neuroimage.2013.05.050

Tzourio-Mazoyer N, Landeau B, Papathanassiou D et al (2002) Automated anatomical labeling of activations in SPM using a macroscopic anatomical parcellation of the MNI MRI single-subject brain. Neuroimage 15:273–289. https://doi.org/10.1006/nimg.2001.0978

van Kesteren MTR, Fernandez G, Norris DG, Hermans EJ (2010) Persistent schema-dependent hippocampal-neocortical connectivity

during memory encoding and postencoding rest in humans. Proc Natl Acad Sci 107:7550–7555. https://doi.org/10.1073/pnas.0914892107

Yassa MA, Stark CEL (2011) Pattern separation in the hippocampus. Trends Neurosci 34:515–525